

Unsupervised learning universal critical behavior via the intrinsic dimension

T. Mendes-Santos^{*},¹ X. Turkeshi^{*},^{1,2,3} M. Dalmonte,^{1,2} and Alex Rodriguez¹

¹*The Abdus Salam International Centre for Theoretical Physics, strada Costiera 11, 34151 Trieste, Italy*

²*SISSA, via Bonomea, 265, 34136 Trieste, Italy*

³*INFN, via Bonomea, 265, 34136 Trieste, Italy*

The identification of universal properties from minimally processed data sets is one goal of machine learning techniques applied to statistical physics. Here, we study how the minimum number of variables needed to accurately describe the important features of a data set - the intrinsic dimension (I_d) - behaves in the vicinity of phase transitions. We employ state-of-the-art nearest neighbors-based I_d -estimators to compute the I_d of raw Monte Carlo thermal configurations across different phase transitions: first-, second-order and Berezinskii-Kosterlitz-Thouless. For all the considered cases, we find that the I_d uniquely characterizes the transition regime. The finite-size analysis of the I_d allows not just to identify critical points with an accuracy comparable with methods that rely on *a priori* identification of order parameters, but also to determine the class of the transitions and to access the corresponding (critical) exponents. For the case of topological transitions, this analysis overcomes the reported limitations affecting other unsupervised learning methods. Our work reveals how raw data sets display unique signatures of universal behavior in the absence of any dimensional reduction scheme, and suggest direct parallelism between conventional order parameters in real space, and the intrinsic dimension in the data space.

I. INTRODUCTION

The growing field of machine learning (ML) is rapidly expanding our capabilities of analyzing and describing high-dimensional data sets [1–4]. With the increasing understanding of these methods, the community is becoming convinced that their outstanding performance is mostly due to the fact that this “high-dimensionality” is applicable only to the embedding space, while the data sets lay in a manifold that can be twisted and topologically complex but whose intrinsic dimension, I_d , is typically much smaller than the large number of coordinates of the system [5, 6] (see graphics in Fig. 1 (A)). The determination of this I_d is an active field of research [5, 7, 8] in unsupervised learning (UL), i.e., the branch of machine learning that aims to uncover the internal structure of a data set without the need of any label.

Recently, ML ideas have encountered fruitful applications in the context of statistical physics [9–11]. Such applications have ranged from the determination of physical properties [12–19], to the formulation of novel classes of variational ansätze [20–23]. These progress leveraged on analyzing and exploiting the results of dimensional reduction, and employing a variety of tools to analyze (or employ) the final representation (or truncation) obtained in this way. In various contexts, results obtained via these methods have remarkably shown to be already competitive with more traditional approaches [9].

Here, we pursue an alternative approach: our main purpose is to show that, from a ML perspective, physically relevant and universal information can be gathered by analyzing the very same embedding procedure that

carries out the dimensional reduction, rather than focusing on its final result. In particular, we show how the intrinsic dimension correspondent to the partition function of statistical mechanics models displays universal scaling behavior in the vicinity of phase transitions, and it works as an order parameter for a corresponding structural transition in data space. Differently from previous works [12, 24–30], our approach is thus focused on *data mining* the data set as a whole, and thus, does not leverage on any kind of projection. At the technical level, this is achieved by employing a cutting-edge nearest-neighbor estimator of the I_d , which is suitably designed to deal with non-linear data sets [8].

In order to access the complex data structure at phase boundaries, we study numerically instances of first-order, second-order (conformal), and Berezinskii-Kosterlitz-Thouless (BKT) transitions in two-dimensional (2D) classical spin systems. In all cases, I_d displays a universal scaling behavior correspondent with the transition properties of the underlying lattice model. (i) For first-order transitions, I_d peaks at the critical point due to the coexistence of different orders, and the finite-size corrections of the transition temperature are dictated by trivial scaling exponents. (ii) For both second-order and topological transitions, we observe *universal scaling collapse*, with transition temperature and critical exponents determined to the percent level. (iii) Most importantly, we provide compelling evidence that the I_d is an ideal tool to underpin topological transitions in an unsupervised fashion: as an example, we extract the critical temperature of the 2D XY model with 1% confidence even at modest system sizes.

Before diving into the main part of our manuscript, we provide a simplified picture that qualitatively captures how the intrinsic dimension is connected to the physical information obtained by sampling a partition

^{*} Equal contribution.

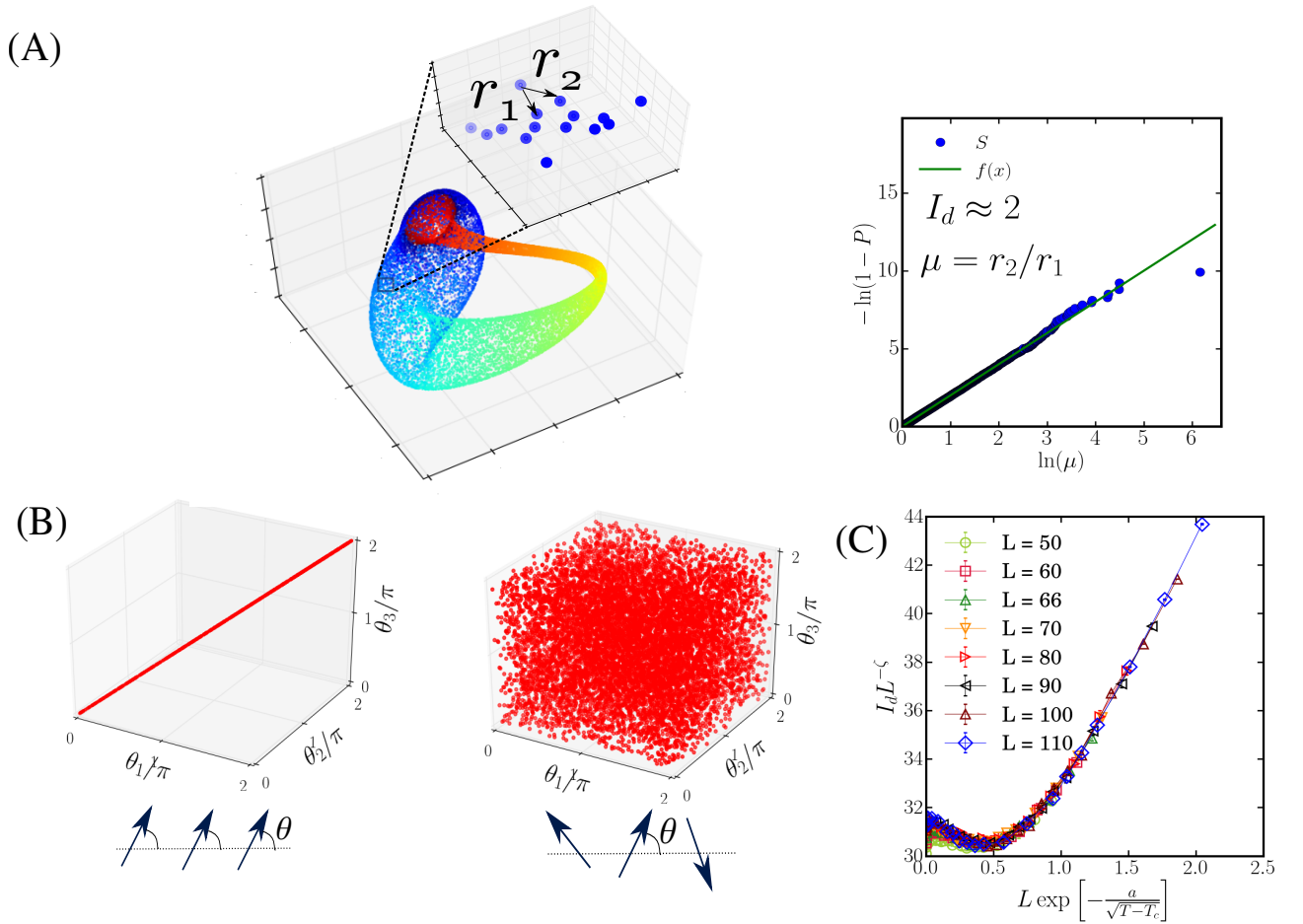


Figure 1. Panel (A): *Schematics of the intrinsic dimension, I_d .* The important content of a data set typically lays in a manifold whose I_d is much lower than the number of coordinates. In the example, despite the synthetic data set (Klein's bottle-shaped) is embedded in a three-dimensional space, it can be effectively described by a twisted manifold whose $I_d = 2$. The key ingredients to compute the I_d are the first- and the second-nearest neighbor distances, r_1 and r_2 , of each point of the data set. The computation of the I_d is based on the fitting of the *empirical* cumulative distribution function (CDF) of the ratio $\mu = r_2/r_1$, $P(\mu)$ [see text and Eq. (1)]. Panels (B): *Low- and high-temperature data sets of a 3-site model in configuration space.* The points represent the 3-site XY model configurations: $\vec{\theta} = (\theta_1, \theta_2, \theta_3)$. The high- and zero-temperature cases show simple data structures: for $T = 100$, I_d is equal to the number of spins, while for $T = 0$, $I_d = 1$. Panel (C): *Intrinsic dimension in the vicinity of a phase transition.* The I_d in the intermediate temperature regime, representative of phase transitions in larger systems, is considerably more complex. The temperature dependence of I_d can be used to signalize and characterize critical points. As an example, we show the universal data collapse of the I_d at the Berezinskii-Kosterlitz-Thouless described by the 2D XY model.

function via Monte Carlo methods. The basic intuition behind the I_d of data sets generated in the low- and high-temperature regimes of a simple 3-site XY model is drawn in Fig. 1 (B). At low temperature (left graphics of Fig. 1 (B)), most of the spin configurations sampled during the Markov chain correspond to fully ferromagnetic spin arrangements (see cartoon). In the limiting case $T = 0$, the ground states are given by XY ferromagnetic configurations, i.e., $\theta_1 = \theta_2 = \theta_3$, and the data set is described by a manifold that lays in a line ($I_d = 1$). Oppositely, in the high temperatures regime, the data set is described by a manifold whose $I_d = 3$: each new Monte Carlo configuration corresponds to an arbitrary arrangement of

the three spins, so that the structure of the data set is that of a homogeneously occupied three-dimensional space. This simple example demonstrate how transitions in parameter space are accompanied by structural transitions in data space. Due to its collective origin, the transition region requires the computation of I_d in very high dimensional data space: in Fig. 1 (C), we show a sample of our results, illustrating the scaling collapse of the intrinsic dimension correspondent of the 2D XY model in the vicinity of its BKT transition point.

II. INTRINSIC DIMENSION

Before diving into the analysis of concrete statistical mechanics models, we present here a self-contained discussion on the intrinsic dimension and its state-of-the-art estimators. This section is propaedeutic to the critical identification of the best estimator to be used in our applications below.

The I_d represents the minimum number of variables needed to describe a data set [7, 8]. Information about the I_d is important to determine if dimensional reduction of high-dimensional data sets incurs information loss or not. Moreover, it can be used as an UL approach to characterize a system. Just to mention a few examples: in biological physics, the I_d can be used to determine the number of independent directions a protein can have during a sequence evolution [31], in image analysis, to distinguish between different kind of image structures [32], in astrophysics, to estimate the amount of information available in spectropolarimetric data [33], in theoretical machine learning, to understand the properties of deep neural networks [34], and in ecology, to characterize the minimum number of independent axes of variation that adequately describes the functional variation among plants [35].

Different approaches have been developed to estimate the I_d , see Ref. [7] for review. For example, dimensional reduction techniques, such as principal component analysis (PCA) [36], Multidimensional Scaling [37], Iso-map [38], Locally Linear Embedding [39], t-distributed stochastic neighbor embedding (t-SNE) [40] or Uniform Manifold Approximation and Projection (UMAP) [41] to mention some of them, search for a lower dimensional space to project the data set by minimizing a projection error. The dimension of the identified subspace is viewed as an estimation of I_d . However, identifying this dimension is far from trivial. For instance, in the PCA case, one should take into consideration the spectrum of the eigenvalues of the covariance matrix and look either for a gap or decide *ad hoc* a cut-off parameter. It is worth saying that, for PCA, this strategy will not work if the manifold of lower dimensionality is curved.

A closely related quantity is the fractal dimension [42], whose estimation relies on the scaling of the number of neighbors with the distance from a given point. This approach is largely employed in the study of percolation transitions [43], but it suffers from serious limitations when the density distribution of points is not uniform.

These limitations lead to the development of nearest neighbors methods, in which it is assumed that nearest-neighborhood points can be considered as uniformly drawn from small enough I_d -dimensional hyperspheres (not all the data set) [5, 7]. Indeed, the avoidance of any projection step and the smoothing on the condition of data uniformity (from the full data set to a small neighborhood around each point) are key features for obtaining good results in highly non-uniform, non-linear data sets even at really high dimensions (a regime at which all

the purely geometrical methods present a bias due to the curse of dimensionality).

The TWO-NN method employed in this work belongs to this type of methods, with the particularity that by focusing only on the first two nearest neighbors (see Fig. 1 A), the size of the I_d -dimensional hyperspheres at which the density is assumed constant is reduced to its minimum expression. The method is rooted in computing the distribution functions of neighborhood distances, which are function of I_d . More specifically, for each point \vec{x} in the data set, we consider its first and second nearest-neighbors distances $r_1(\vec{x})$ and $r_2(\vec{x})$, respectively. Under the condition that the data set is locally uniform in the range of second nearest-neighbors, it has been shown in Ref. [8] that the distribution function of $\mu = r_2(\vec{x})/r_1(\vec{x})$ is $f(\mu) = I_d \mu^{-I_d-1}$. Or, in terms of the cumulative distribution, $P(\mu)$,

$$I_d = -\frac{\ln[1 - P(\mu)]}{\ln(\mu)}, \quad (1)$$

which can be used to obtain I_d by fitting $S = \{(\ln(\mu), -\ln[1 - P^{\text{emp}}(\mu)])\}$ with a straight line passing through the origin. The function P^{emp} defines the empirical cumulate and is computed by sorting the values of μ in an ascending order, see Appendix A for more details. In Fig. 1 A, the steps for computing the I_d in a highly non-linear manifold with complex topology (in this case, a Klein's bottle-shaped data set) are summarized: a) Compute the distance from the first and second neighbors b) Compute for each point μ and its empirical cumulate and c) fit S to a straight line.

We stress that this method is not free of drawbacks. As mentioned above, being a purely geometrical method, it is affected by the curse of dimensionality, since the number of points needed to have an accurate measure of the I_d grows exponentially with the I_d . Moreover, Equation (1) was derived assuming a continuous real support. Therefore, applying it to data sets with a different support implies some degree of approximation that can fail in some limiting cases. For instance, this shall happen when two or more configurations have the same coordinates. However, as we detail below, these drawbacks do not affect the results obtained in this work: in particular, these limitations do not kick in when investigating transitions, even when configuration spaces are composed of discrete variables such as Ising spins. These limitations only affect data sets corresponding to either very small system sizes, or phases at extremely low temperatures where, during the MC sampling, configurations may be repeated as the accessible configuration space is very simple.

III. MODELS

Our approach focuses on the high-dimensional data sets associated with the equilibrium configuration states of a partition function. Such states are sampled with

Markov Chain Monte Carlo simulations from the thermal weight $\rho(E) \sim e^{-E(\vec{x})/T}$, where $E(\vec{x})$ is the energy of an independent configuration \vec{x} and T is the temperature. We employ Wolff's cluster algorithm [44, 45], and for each data set, we consider N_r configurations.

We consider partition-function data sets of several models in the vicinity of various types of phase transitions [46, 47]. The first example is the well known Ising model in two-dimensions

$$E(\vec{s}) = - \sum_{\langle i,j \rangle} s_i s_j, \quad (2)$$

where the spin degrees of freedom are $s_i = \pm 1$, and $\langle i, j \rangle$ are the nearest neighboring bonds of a square lattice, with $N_s = L \times L$ spins and periodic boundary condition. The Ising configuration states are defined as

$$\vec{s} = (s_1, s_2, \dots, s_{N_s}). \quad (3)$$

This model describes a second-order phase transition characterized by the breaking of a Z_2 symmetry at the critical temperature $T_c = 2/\ln(1+\sqrt{2})$. In the vicinity of T_c , the spin correlation length diverge as $\xi \sim (T - T_c)^{-\nu}$, where the critical exponent is $\nu = 1$.

We also consider the first- and second-order phase transitions described by the q -states Potts model (qPM)

$$E(\vec{\sigma}) = - \sum_{\langle i,j \rangle} \delta_{\sigma_i, \sigma_j}, \quad (4)$$

where the spin $\sigma_i = 0, 1, 2, \dots, q-1$, and $\delta_{\sigma_i, \sigma_j}$ is the delta function. In particular, the $q = 2$ Potts model can be mapped into the Ising model. The Potts configuration states are defined by

$$\vec{\sigma} = (\sigma_1, \sigma_2, \dots, \sigma_{N_s}). \quad (5)$$

The qPM is characterized by a discrete Z_q symmetry that is broken at the critical temperature $T_c = 1/\ln(1 + \sqrt{q})$. Importantly, this class of models displays a second-order phase transition for $q \leq 4$, and a first-order one for $q > 4$. We examine both these regime: the second-order transition described by the $q = 3$ PM (with correlation length critical exponent $\nu = 4/5$), and the first-order transition described by the $q = 8$ PM [48, 49].

Finally, as a representative of the BKT universality class, we investigate the two-dimensional XY model[50, 51]

$$E(\vec{\theta}) = - \sum_{\langle i,j \rangle} \vec{S}_i \cdot \vec{S}_j, \quad (6)$$

where $\vec{S}_i = (\cos(\theta_i), \sin(\theta_i))$, $\cos(\theta_i)$ and $\sin(\theta_i)$ being the projection of the spin at site i in the x and y directions, respectively, and $\theta_i \in [0, 2\pi[$. The XY configurations are defined as

$$\vec{\theta} = [\cos(\theta_1), \sin(\theta_1), \dots, \cos(\theta_{N_s}), \sin(\theta_{N_s})], \quad (7)$$

This model is characterized by a continuous $U(1)$ symmetry and describes a phase transition between a high-temperature phase with exponentially decaying spin correlations, and a low-temperature quasi-ordered phase characterized by power-law decaying correlations. The BKT critical temperature, T_{BKT} , is not known exactly; state-of-the-art estimations based on the analysis of the spin stiffness of lattices of order $O(10^6)$ spins give $T_{BKT} = 0.8935(1)$ [52].

The detection of the BKT critical point is hindered by the fact that it cannot be characterized by conventional local order parameters, as in the examples discussed previously, and due to the exponential growth of the correlation length near T_{BKT} . Hence, the BKT transition represents a key challenging test for any UL method.

A. How to characterize partition functions as data sets

Before proceeding to the discussion of the results, we point out some important aspects of the Ising, Potts and XY data sets (see Eqs. (3), (5) and (7), respectively). First, a crucial step to obtain the I_d (cfr. Eq. (1)) is to consider a proper metric; the distance $r(\vec{x}^i, \vec{x}^j)$ between two configuration states \vec{x}^i and \vec{x}^j must be non-negative, equal to zero only for identical configurations, symmetric, and satisfy the triangular inequality.

For the XY data sets the distance is defined as the the Euclidean distance:

$$r(\vec{\theta}^i, \vec{\theta}^j) = \sqrt{2 \sum_{k=1}^{N_s} (1 - \vec{S}_k^i \cdot \vec{S}_k^j)}. \quad (8)$$

This distance properly takes into account the periodicity of the configuration states in the interval $\theta_i \in [0, 2\pi[$.

For both Ising and Potts configuration states, we consider the Hamming distance, i.e., $r(\vec{s}^i, \vec{s}^j)$ (or $r(\vec{\sigma}^i, \vec{\sigma}^j)$) is given by the number of positions in the state vectors (\vec{s}^i and \vec{s}^j) for which the corresponding coordinates are different. The choice of the Hamming distance is motivated by the fact that the energy difference between two spins in the model of interest is given by a delta function.

As mentioned in the previous section, the two-NN method fails when two or more sampled configurations of the data set have identical coordinates. This issue typically occurs in the discrete-variables Ising and Potts data sets, when the total number of independent configuration states, N_c , is smaller or of the same order of the number of configurations used in the data set, N_r . For instance, for both Ising and Potts data sets, identical ferromagnetic configurations are sampled in most of the Monte Carlo steps when $T \ll T_c$. However, in the regime that we focus here (i.e., T close to T_c and $L > 10$), as $N_c \gg N_r$, this issue is irrelevant (we have explicitly checked this in our data sets).

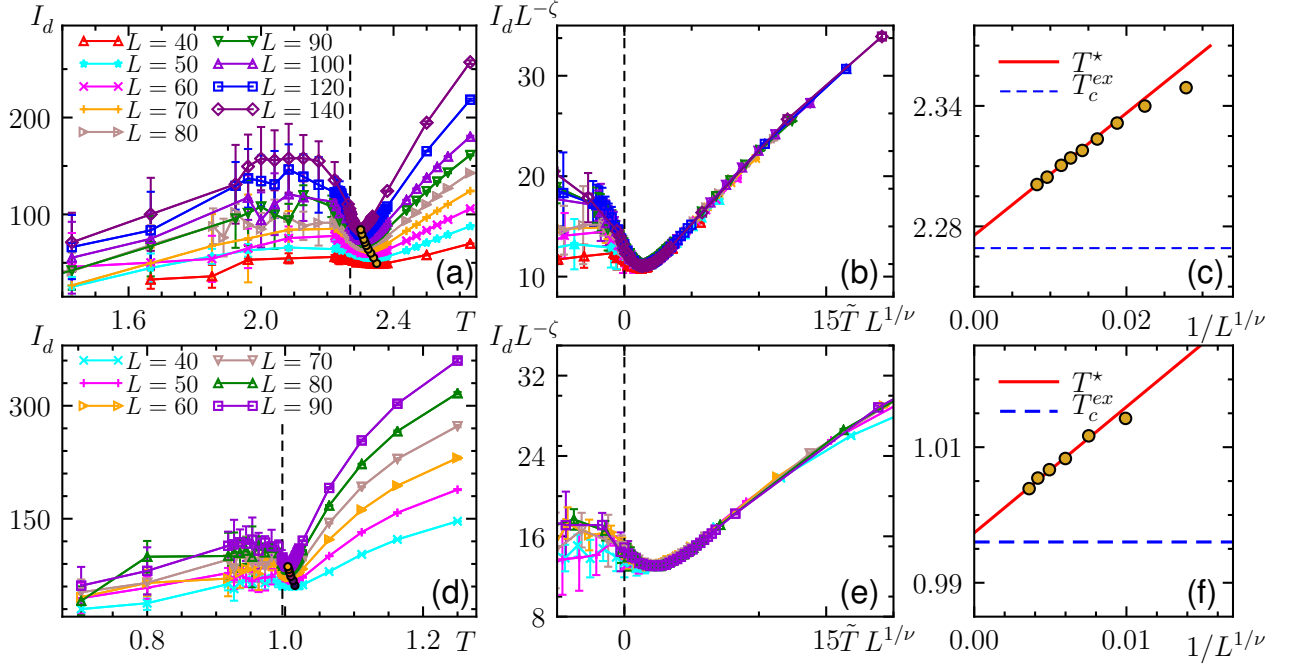


Figure 2. *Second-order phase transition.* Panels (a-c): Ising model. Panels (d-f): $q = 3$ Potts model. Panels (a,d): I_d as a function of T for the Ising model. Errorbars are standard deviation associated to a distributions of n realizations of I_d (we typically consider $n \geq 5$). Panel (b,e): data collapse of I_d based on the FSS discussed in main text. The best data collapse of the results give $T_c = 2.283(2)$, $\nu = 1.02(2)$ and $\zeta = 0.410(5)$ for the case of the Ising model, and $T_c = 0.996(2)$, $\nu = 0.805(5)$, and $\zeta = 0.420(2)$ for the case of the Potts model. Panels (c,f): finite size (FSS) scaling of the minimum temperature T^* (see text); the horizontal line is the exact result for T_c . The extrapolation returns $T_c = 2.2784(2)$ and $T_c = 0.9970(3)$ for the Ising and Potts cases, respectively.

Finally, we mention that data sets generated by the XY configuration states are typically nonlinear, which can be noted by the fact that linear dimension reduction methods, such as PCA, fails to describe XY data sets, see Ref. [28]. In fact, even for the simple data set shown in Fig.1 (B), linear PCA fails in estimating the true I_d of the system when the proper distance between the configurations are taken into account, see the Appendix A. This feature of the XY data sets reveals the necessity of using state-of-the-art I_d -estimators (such as the two-NN method considered here) that properly takes into account nonlinearities.

IV. RESULTS

A. Second-order phase transitions

We start our discussion considering the second-order phase transitions (2PTs) described by the Ising and the 3-states Potts (3PM) models, see Fig. 2. We consider data sets formed by $N_r = 5 \times 10^4$ configuration states. Overall, far from the transition, I_d is an increasing function of T . For low- T , the computation of I_d is affected by the discreteness of the Potts (Ising) configurations; which

reflects on the larger error bars. However, this issue is mitigated close to the critical point, T_c . Remarkably, I_d exhibit a non-monotonic behavior in the vicinity of the critical point (see Figs. 2 (a1) and (b1)) which can be used to locate and characterize the transition point itself.

As is conventionally done in the analyses of physical observables, e.g., magnetic susceptibility and heat capacity, we now consider a finite-size scaling (FSS) theory for I_d . First, based on the FSS hypothesis and postulating that I_d behaves as a true order parameter for the transition, one has $I_d = L^\zeta f(\xi/L)$, where the correlation length diverges as $\xi \sim (T - T_c)^{-\nu}$, ν is a critical exponent, and ζ is a scaling exponent associated with the divergence of I_d at T_c . Figs. 2 (a2) and (b2) show the universal data collapse for Ising and 3PM, respectively. The values obtained for T_c and ν have a discrepancy with exact results of less than 0.5% and 4%, respectively. For Ising we obtain: $T_c = 2.283(2)$, $\nu = 1.02(2)$, and $\zeta = 0.410(5)$, while for 3PM: $T_c = 0.996(2)$, $\nu = 0.805(5)$, and $\zeta = 0.420(2)$. See the Appendix C, for the discussion about the details of the data-collapse procedure.

Further, we consider the size scaling of the shift of the local minimum of $I_d(T)$ (i.e., the temperature $T^*(L)$),

$$T^*(L) - T_c \sim \frac{1}{L^{1/\nu}}. \quad (9)$$

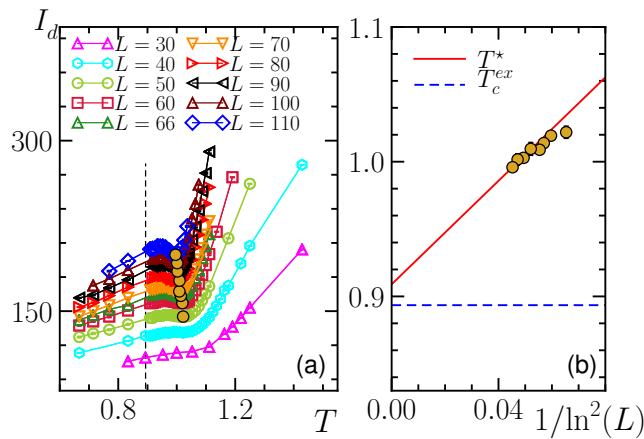


Figure 3. *Berezinskii-Kosterlitz-Thouless transition*. Panel (a) shows the temperature dependence of I_d for different values of L . The dashed line indicates the value of the BKT critical temperature obtained in Ref. [52] using conventional methods, $T_{BKT} = 0.8935(1)$. For each point, we harvested approximated 10 instances of the data set and average the resulting estimates for the I_d . The error bars are the standard deviation of such set of results. The scaling collapse obtained with these data sets is depicted in Fig. 1 (c). Panel (b) shows the finite-size scaling of T^* based on Eq. (10). Fitting the results for $L = 80, 90, 100$ and 110 , we obtain $T_{BKT} = 0.909 \pm 0.015$. In the text, we discuss how we obtain the local minimum of I_d , T^* . We compute the I_d of manifolds with $N_r = 5 \times 10^4$ configurations.

We note that $T^*(L)$ is reminiscent of the universal scaling behavior of singular features of physical observables close to T_c (e.g., the peak of the magnetic susceptibility) [53]. In order to compute T_c , we employ the following procedure: (i) we obtain $T^*(L)$ by fitting the results in an interval close to $T^*(L)$ with a cubic function; the fitting is performed with a jackknife procedure, which allows establishing an error bar for $T^*(L)$. We then (ii) consider the aforementioned FSS to compute T_c ; the fitting is performed considering different sets of points. This method provides a coherent error propagation for T_c . We obtain, $T_c = 2.2784(2)$ for the Ising model and $0.9970(3)$ for the 3 state Potts model. Their discrepancies with the exact values are respectively of order 0.4% and 0.2%.

The results of this analysis confirm the validity of our original assumption, that is, that the intrinsic dimension is a valid order parameter describing the transition in data space as a structural transition. We remark that this is validated at two steps - firstly, via the quality of the scaling collapse, and secondly, by the scaling of the transition temperature obtained by analysis a single feature of the I_d dependence with respect to the temperature. Those represent two fundamental tests that any valid order parameter shall satisfy at transition points.

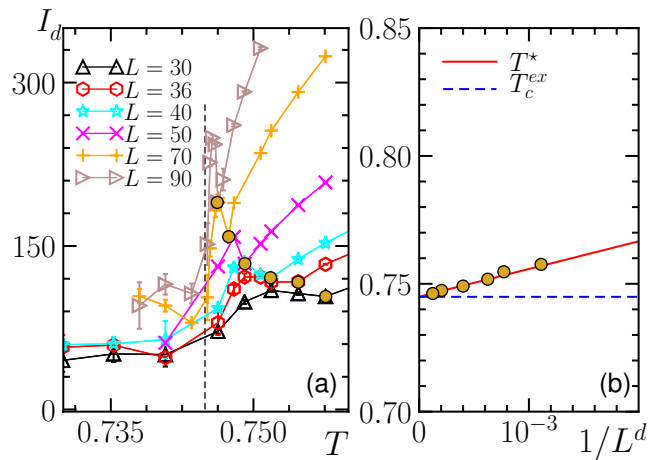


Figure 4. *First-order phase transition*. Panel (a) shows I_d as function of T for the 8-states Potts model. Panel (b) shows the finite size (FSS) scaling of T^* , where $d = 2$ (see text).

B. Berezinskii-Kosterlitz-Thouless (BKT) phase transition

Unsupervised learning of phase transitions associated with the break of a discrete symmetry, as discussed in the previous section, can also be performed with PCA [12, 26, 54]. For example, the critical temperature of the Ising model can be obtained with an accuracy similar to the ones obtained here. PCA is based on a linear dimension reduction, and thus, differs on a fundamental way from our unsupervised approach, which is based solely on the analysis of the I_d . Furthermore, as we discuss in this section, our approach can be extended to cases that PCA does not work, such as the topological BKT phase transition.

The difficulties in learning the BKT transition from raw XY configurations occur in both supervised [55] and unsupervised [26] ML approaches. In the latter case, it is related to the fact that manifolds generated by XY configurations are usually curved. Recent progress based on diffusion maps [28, 56] or topological data analysis [57] have been made to solve this problem, typically considering problem-specific insights (such as the structure of topological excitations). These approaches have shown how considerable qualitative insight can be gathered on the nature of the BKT transition. However, it is presently unclear if the raw data structure corresponding to topological transitions can exhibit universal features, and if so, if unsupervised approaches can be used to detect the critical temperature with an accuracy that is comparable with conventional methods (that typically rely on the a priori knowledge of the order parameter).

In Fig. 3 (a), we show the temperature dependence of I_d in the transition region. The intrinsic dimension clearly distinguishes the low- T regime, characterized by bound vortex-antivortex pairs, from the unbinding high-

T regime. In the vicinity of the BKT critical point, T_{BKT} , the behavior of I_d resembles the one observed for the second-order phase transitions, i.e., I_d exhibit a local minimum at $T^*(L)$ (observed for $L > 30$), which is a signature of the BKT transition. Note that the minimum is clearly visible already for lattices of order $L = 50$; at these sizes, the spin stiffness is instead featuring a very smooth behavior, and considerably larger systems are required to appreciate a qualitative jump in the latter.

We consider the conventional FSS for BKT transition, $I_d(T, L) = L^\zeta f(\xi(T)/L)$, where the singular value of the correlation length diverge exponentially, i.e., $\xi \sim \exp(a/\sqrt{T - T_c})$. In Fig. (1) (C), we show the universal data collapse for different values of L , where a , T_{BKT} and ζ are treated as free-parameters in the collapse procedure; see the Appendix C. The value obtained, $T_{BKT} = 0.92(1)$, is in good agreement with estimations of T_{BKT} obtained on Ref. [53].

A more accurate estimation of T_{BKT} is based on the finite-size scaling of $T^*(L)$. This approach relies on the computation of $T^*(L)$, which is performed with the same procedure described in the previous section, and the finite size scaling ansatz [53]:

$$T^*(L) - T_{BKT} \sim \frac{1}{\ln^2 L}. \quad (10)$$

As discussed before this procedure allows us to establish an error bar for the calculated T_{BKT} . We obtain $T_{BKT} = 0.909 \pm 0.015$, that is compatible within error bars with Ref. [52] where simulations with up to $O(10^6)$ spins were carried out. For comparison, the best alternative method [28] utilizing unsupervised learning techniques reported relative errors of the order of 5%.

Conventionally, T_{BKT} is obtained with the aid of the so-called Nelson-Kosterlitz universal jump of the spin wave stiffness [58], which allows to determine the finite-site critical temperature, $T_{BKT}^*(L)$. The FSS [Eq. (10)] is then used to determine BKT critical point at the thermodynamic limit. Remarkably, here we observe that the intrinsic dimension of raw XY data sets exhibit a clear signature of the finite-site T_{BKT} , even for moderate system sizes we have considered.

C. First-order phase transitions

Finally, we consider an example of first-order phase transition (1PT): the 8-state Potts model (8PM). As is typical of 1PT the system exhibit a finite-size correlation length at T_c , $\xi_8 = 23.9$ [59]. For $L > \xi_8$, the transition can be described by trivial and generic critical exponents, e.g., $\nu = 1/d$, d being the system dimension [49, 60, 61]. Furthermore, the finite-size shift of the critical temperature, $T_c(L)$, conventionally detected, for example, by the maximum value of the magnetic susceptibility, scales as $T_c(L) - T_c \sim 1/L^d$.

Fig. 4 shows that I_d also exhibit a clear signature of the 1PT, featured by a peak at T_c for $L \gg \xi_8$. For

$L \approx \xi_8$, the temperature dependence of I_d resembles the one observed for 2PTs in Fig. 2; i.e., I_d exhibit a local minimum at a temperature T^* . Interesting, the FSS of T^* is in agreement with first-order transitions, see Fig. 4 (b) [60, 61]; the discrepancy of the calculated $T_c = 0.7448(1)$ with the exact value is less the 0.05%

V. DISCUSSION

Our results so far support the fact that, in the vicinity of a phase transition, the intrinsic dimension behaves as an order parameter for both first, second-order and BKT transition, and this order parameter is tight to a transition between different data structures in configuration space. Within this framework, the position of the transition is always identified with the scaling of the minimum of the intrinsic dimension. We now provide a qualitative discussion in support of this picture.

In continuous phase transitions, collective behavior is captured by only a handful of parameters. This suggests that the amount of information required to describe the system is parametrically simpler at the critical point when compared to its vicinity, as the latter region requires additional information on the operators required to perturb away from criticality. This emergent simplicity may have several consequences at the data structure level. The most simple consequence is that one expects a simplified data structure to be described by a minimum of the intrinsic dimension at the transition point. This is exactly what we have observed at both second-order and BKT transitions. We note that this expectation is not related to the number of states sampled by the partition function (this number is, in our case, fixed by N_r are configurations are never repeated). The discussion of how our results change with N_r is reported in Appendix B.

For first-order transitions, the above reasoning is not applicable as it relies on universal behavior, and thus the existence of a continuum limit. In these cases, one expects that the data space in the vicinity the transition point shall feature two separate regions, each of them composed of states representing the two phases meeting at T_c . Exactly at the transition point, one expects an abrupt change in the data structure: indeed, the MC sampling will access a large number of configurations corresponding to both phases (in analogy to metastability), and thus display a sharp increase (see Fig. 4 (a)). Approaching the transition point from the disordered phase will feature instead of a minimum, that scales to the transition point.

The arguments above serve as a qualitative guideline behind the basic picture we put forward: the simplified field theory description applicable at transition points reflects directly into the data structure of the problem. We believe this picture to be correct in view of our results above, and in particular, in view of the quality of the scaling collapses obtained. At the methodological level,

it would be an interesting future work to develop an analytical understanding of this fact, based on the very close analogy between the intrinsic dimension and fractal dimensions in structural transitions.

We note that the systems sizes where the intrinsic dimension starts featuring a clear minimum structure are very similar in the case of both second-order and BKT transitions (in the case of first-order, the minimum structure appears once sizes of the order of the correlation length are reached, in agreement with the discussion above). This behavior is quite different from the one of conventional one- or two-point correlation functions, whose characteristic features are typically appearing at very different system sizes for transitions belonging to different universality classes. Indeed, by focusing on the geometrical and 'curvature' attributes of the data, the emerging of the features of the intrinsic dimension depends mostly on the characteristics of the data set of configurations (for instance, the number of data points or the dimension of embedding space). Therefore, these features appear at similar system sizes when the data space is similar, independently of the class of transition.

We also note that, in comparison with previous applications in other fields [31, 34, 62], the values of the intrinsic dimension reported here are considerably larger. For future applications, like combining our analysis with clustering methods that do not rely on dimension reduction[63], it may be interesting to develop novel estimators that focus on large values of I_d , potentially trading absolute accuracy with numerical efficiency.

VI. CONCLUSIONS

We have shown that phases transitions can be learned through a single property of raw data sets of configurations - the intrinsic dimension - without any need to perform dimensional reduction. The key observation made here is that, in analogy to physical observables, the intrinsic dimension exhibits universal scaling behavior close to different classes of transitions: first-, second-order, and Berezinskii-Kosterlitz-Thouless (BKT). This indicates how the intrinsic dimension serves as an order parameter in data space, showing how the latter undergoes a structural transition that parallels the phase transition identified by conventional order parameters.

At the practical level, we have shown that the finite-size analysis of intrinsic dimension allows not just to detect, but also to characterize critical points in an unsupervised manner. In particular, we have shown that the intrinsic dimension allows one to estimate transition temperatures and (critical) exponents of both first- and second-order transitions with accuracies ranging from 1% to 0.1% at very modest system sizes. In addition, the method is equally applicable to topological transitions, where we have demonstrated an accurate (with 1% of confidence) estimation of the BKT topological transition competitive with more traditional methods at the same

system sizes. This latter result suggests that the lack of any dimensional reduction allows retaining topological information in the vicinity of the phase transition, which may instead be lost otherwise [26, 28].

A fundamental aspect of our approach is that it is based on a I_d -estimation method suitable to learn complex manifolds, such as the twisted XY manifold emerging at the BKT critical point. The results demonstrate the potential of state-of-the-art I_d -estimators [8] methods to tackle many-body problems, and motivates an even stronger methodological connection between data mining techniques, and many-body physics.

Some of the methods presented here may be applied to quantum mechanical objects, such as quantum partition functions, density matrices, and wave functions. It is an open challenge to determine whether the data mining of quantum objects can provide an informative perspective on the latter, such as, e.g., accessing entanglement or other more challenging forms of quantum correlations. Finally, while we focused on configuration generated by Monte Carlo sampling, our approach is equally applicable to experimentally generated data; it may be interesting to apply it to settings where raw data configurations are available, such as, e.g., quantum gas microscope experiments [18, 64, 65].

VII. ACKNOWLEDGEMENTS

We acknowledge useful discussions with R. Ben Ali Zinati, R. Fazio, A. Laio and R. T. Scalettar. The work of TMS, XT and MD is partly supported by the ERC under grant number 758329 (AGEnTh), by the Quanterra programme QTFLAG, and has received funding from the European Union's Horizon 2020 research and innovation programme under grant agreement No 817482. This work has been carried out within the activities of TQT. TMS and XT acknowledge computing resources at Cineca Supercomputing Centre through the Italian SuperComputing Resource Allocation via the ISCRA grants ICT20_CMSP and MLforPT.

Appendix A: The TWO-NN method and comparison with principal component analysis (PCA)

In this section, we provide more details about the two-NN method. As described in Ref. [8], the intrinsic dimension, I_d , can be obtained through the following steps:

1. For each point i of the data set ($i = 1, 2, \dots, N_r$), compute its first- and second-nearest neighbor, $r_1(i)$, $r_2(i)$, respectively.
2. For each point i , compute the ratio $\mu_i = r_2(i)/r_1(i)$.
3. The empirical cumulate is defined as $P^{\text{emp}}(\mu) = i/N_r$, while the values of μ_i are sorted in

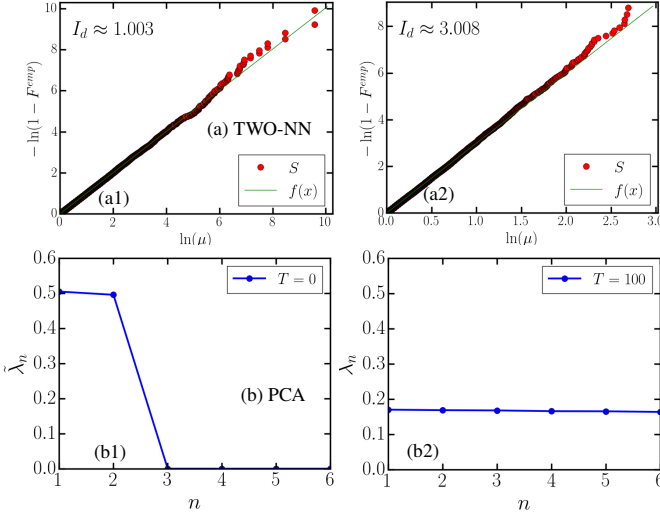


Figure 5. *3-site XY model*. Panels (a) show results of the TWO-NN method: fitting of the data points S for (a1) $T = 0$ and (a2) $T = 100$. The data set have $N_r = 10^3$ configurations. We obtain (a1) $I_d = 1$ and (a2) $I_d = 3$. Panels (b) show results of the PCA method: normalized eigenvalues of the covariance matrix, $\tilde{\lambda}_n$, obtained from the raw XY configurations. Here we use the same notation of ref. [26] For $n > I_d^{\text{PCA}}$, $\tilde{\lambda}_n \rightarrow 0$. PCA predicts (b1) $I_d^{\text{PCA}} = 2$ and (b2) $I_d^{\text{PCA}} = 6$, which is not in agreement with the exact results (see text)

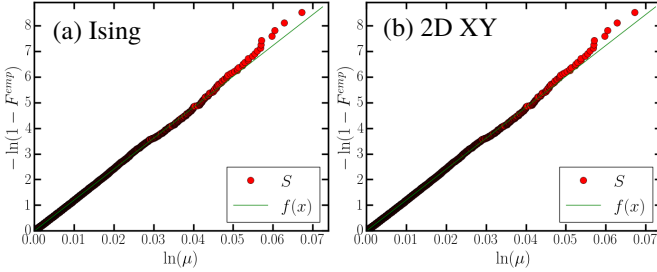


Figure 6. Results of the TWO-NN method: fitting of the data points S for (a) Ising and (b) 2D XY thermal data sets generated close to the critical point (in (a) $T \approx 2.2$, while in (b) $T \approx 0.89$); in both cases we consider $L = 40$, and the data set have $N_r = 10^4$ configurations. We obtain $I_d \approx 47$ and $I_d \approx 120$, respectively.

an ascending order through a permutation, i.e., $(\mu_1, \mu_2, \dots, \mu_{N_r})$, where $\mu_i < \mu_j$, for $i < j$.

4. Finally, the resulting $S = \{(\ln(\mu), -\ln[1 - P^{\text{emp}}(\mu)])\}$ are fitted with a straight line passing through the origin. The slope of this line is equal to I_d (see Eq.(1)).

Fig. 5 shows the plot of S for the basic 3-site XY example presented in the Fig. 1 (B). It worth mentioning that while we depict the configurations $\vec{\theta} = (\theta_1, \theta_2, \theta_3)$

for clarity of illustration in Fig. 1 (B), in our calculations, $\vec{\theta}$ is defined as in Eq. (7). In this way, the distance between two configurations $\vec{\theta}^i$ and $\vec{\theta}^j$: $r(\vec{\theta}^i, \vec{\theta}^j) = \sqrt{2 \sum_{k=1}^{N_s} (1 - \vec{S}_k^i \cdot \vec{S}_k^j)}$, properly takes into account the periodicity of the variables θ_k^i . Another important technical aspect is that the fit of S is unstable for larger values of μ . As is considered in ref. [8], we discard the 10% of points characterized by the highest values of μ . Based on this approach, we obtain $I_d \approx 1$ and $I_d \approx 3$, for the zero and high temperature regimes, respectively, which is consistent with the value expected from physical reasonable assumptions (see Figs. 5 (a1) and (a2)).

In contrast, simple linear dimension reduction methods, such as Principal Component Analysis (PCA), fails to describe the I_d of the XY data sets. To illustrate this point, we employ linear PCA in the same collection of configurations considered in the last paragraph. As can be seen from Figs. 5 (b1) and (b2), even for this simple example, PCA fails to obtain the true I_d ; for $T = 0$, $I_d^{\text{PCA}} = 2$, while for $T = 100$, $I_d^{\text{PCA}} = 6$. This failure is related to the fact that the XY manifolds are curved [28].

We also show some examples of the plot of S for data sets generated in the vicinity of the critical points of the Ising and 2D XY models, see Fig. 6 (a) and (b), respectively. In both cases, the points S are well fitted by a straight line passing through the origin. We obtain similar results for the other system-sizes and values of T considered in this work.

Appendix B: Scaling of the I_d with the number of configurations

In this section we discuss the scaling of the I_d with the number of configurations, N_r , considered in the data set; for all the results shown in the main text, $N_r = 5 \times 10^4$. The first important aspect to consider is that the TWO-NN is a scale-dependent method. In other words, the estimation of the I_d is performed on a length scale that is related to the first and second neighbor distances of each point. Thus, by varying N_r , one is probing a different neighborhood size like, i.e., estimating I_d in different scales [8].

To illustrate how this change in scale affects the I_d of the thermal data sets considered here, we first consider the 3-site XY model in Fig. 7 (a). For $T = 1$, the I_d converges to 3 as expected for the high-temperature regime of this model. In the low temperature regime $T \approx 10^{-6}$, however, $I_d(N_r)$ exhibit a plateau at $I_d = 1$ for $N_r \in [10^0, 10^3]$. As illustrate in Fig.1 (B) this simple data set is well described by a one-dimensional manifold. This plateau in $I_d(N_r)$ is a signature of this soft direction [8]. Nevertheless, by further increasing N_r , the I_d increases ($I_d \rightarrow 3$ in this case), as an effect of the decrease of the scale in which I_d is estimated. In this scale regime, the number of soft directions cannot be determined. We stress that the computation of the I_d of the

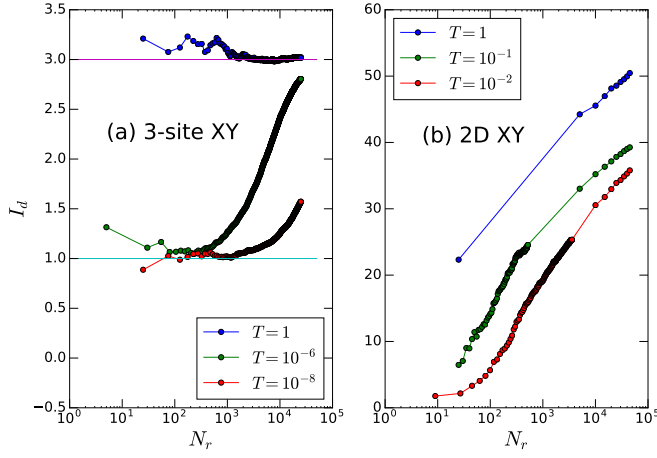


Figure 7. Scaling of the I_d with the number of configurations in the data set. In panel (a) is shown the results for the 3-site XY model, while in panel (b) for the 2D XY model with $L = 10$.

high-dimensional data sets considered here is always performed in this regime. In this case, the I_d exhibit an exponential scaling with N_r , as exemplified in Fig. 7 (b).

We now discuss how the temperature dependence of I_d is affected by the change in N_r . Fig. 8 (a1) and (b1) shows $I_d(T)$ for different values of N_r for the Potts and 2D XY data sets, respectively. Despite the change of the absolute value of I_d with N_r , the qualitative behavior of $I_d(T)$ is not modified. Most importantly, we observe that the position of the local minimum at T^* does not shift with N_r for $N_r > 10^4$. Furthermore, as expected, the scaling of I_d with N_r is exponential, see Figs. 8 (a2) and (b2), at least in the vicinity of the phase transition. Similar results are obtained for other system sizes and for the Ising model. Summing up, our results indicate that, as long as $N_r > 10^4$, the universal scaling behavior exhibited by the I_d is not affected by the scale in which the I_d is measured.

Appendix C: Data collapse

In this section we discuss the finite size analysis employed for the estimates of the critical temperature and exponents presented in Sec. IV. Our procedure is a standard search of the minimal least-square difference fit between our data and an appropriately chosen scaling function hypothesis. Let us first focus on the second-order phase transitions, concerning the Ising and 3-state Potts models. The method is divided into four steps.

- 1 First we choose a suitable mesh for the parameter ranges for T_c , ν and α .
- 2 We compute from our data the scaling variables $x_{\text{dat}}(T_c, \nu) = (T - T_c)L^{1/\nu}$ and $y_{\text{dat}}(\alpha) = I_d(T)L^{-\alpha}$ for different R -range of system sizes $\{L_1, L_2, \dots, L_R\}$.

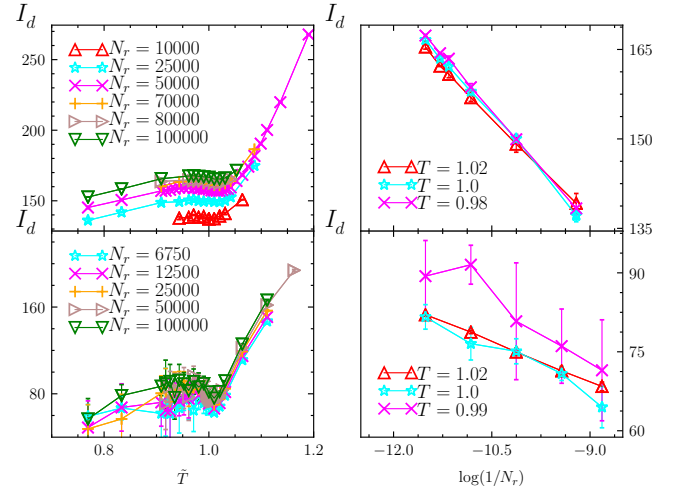


Figure 8. Panels (a): the temperature dependence of the I_d for different values of N_r for the (a1) 2D XY model and (b) 3-states Potts model, in both cases $L = 60$. For each point, we harvested approximated 10 instances of the data set and average the resulting estimates for the I_d . The error bars are the standard deviation of such set of results. Panels (b): the scaling of I_d with N_r for certain values of T .

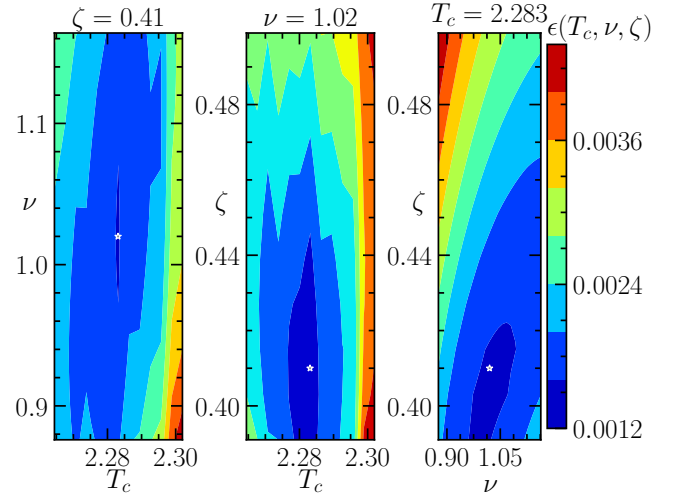


Figure 9. Contour plot of the average residuals projected on the direction of the optimal parameters. The white star points to the optimal parameters for our finite size analysis.

3 We choose a parametric functional hypothesis $f(x; \{a\})$.

4 For each $(x_{\text{dat}}(T_c, \nu), y_{\text{dat}}(\alpha))$ we compute the best fit of the hypothesis function $\{a^*\}$ through the Levenberg-Marquardt algorithm. We store the residuals as:

$$\epsilon(T_c, \nu, \alpha) = \frac{|f(x_{\text{dat}}(T_c, \nu); \{a^*\}) - y_{\text{dat}}(\alpha)|}{|y_{\text{dat}}(\alpha)|} \quad (\text{C1})$$

The optimal set of parameters for each set

$\{L_1, L_2, \dots, L_R\}$ is located in the minimum $\epsilon(T_c, \nu, \alpha)$. In order to keep a low-bias on the hypothesis function $f(x, \{a\})$, we choose various k -degree polynomial $Q_k(x; a_0, a_1, \dots, a_k)$. Thus, we obtain a set of optimal $\{T_c^*\}$, $\{\nu^*\}$, $\{\alpha^*\}$ for each choice of degree k and each set of system sizes $\{L_k\}$. Our estimates and errors for the critical temperature and critical exponents are then estimated as the average and standard deviation of these sets, respectively.

The analysis for the BKT transition (XY model) is performed in a similar fashion. The only difference is the choice of scaling variable, which for this case is:

$$x_{\text{dat}}(T_c, a) = L \exp \left[-\frac{a}{\sqrt{T - T_c}} \right]. \quad (\text{C2})$$

For the Ising, 3-state Potts and XY models we select polynomials of degrees $k \in \{5, 6, 7, 8\}$ and different sets of system sizes among the $L \geq 70$ ones. Our estimations for the XY model are $T_c = 0.92(1)$, $a = 1.4(1)$ and $\zeta = 0.40(1)$.

We visualize the resulting residuals in Fig. 9. Since the parameter space is 3D, for convenience we plot the projected directions along with the optimal critical parameters. Similar considerations hold for the Potts and XY models, although not presented here.

-
- [1] M. I. Jordan and T. M. Mitchell, *Science* **349**, 255 (2015).
 - [2] Y. LeCun, Y. Bengio, and G. Hinton, *Nature* **521**, 436 (2015).
 - [3] P. Domingos, *Communications of the ACM* **55**, 78 (2012).
 - [4] K. T. Butler, D. W. Davies, H. Cartwright, O. Isayev, and A. Walsh, *Nature* **559**, 547 (2018).
 - [5] E. Levina and P. J. Bickel, in *Advances in Neural Information Processing Systems 17*, edited by L. K. Saul, Y. Weiss, and L. Bottou (MIT Press, 2005) pp. 777–784.
 - [6] S. Goldt, M. Mézard, F. Krzakala, and L. Zdeborová, arXiv e-prints, arXiv:1909.11500 (2019), arXiv:1909.11500 [stat.ML].
 - [7] S. Lee, P. Campadelli, E. Casiraghi, C. Ceruti, and A. Rozza, *Mathematical Problems in Engineering* **759567**, 1024 (2015).
 - [8] E. Facco, M. d’Errico, A. Rodriguez, and A. Laio, *Scientific Reports* **7**, 12140 (2017).
 - [9] G. Carleo, I. Cirac, K. Cranmer, L. Daudet, M. Schuld, N. Tishby, L. Vogt-Maranto, and L. Zdeborová, *Rev. Mod. Phys.* **91**, 045002 (2019).
 - [10] P. Mehta, M. Bukov, C.-H. Wang, A. G. Day, C. Richardson, C. K. Fisher, and D. J. Schwab, *Physics Reports* **810**, 1 (2019).
 - [11] J. Carrasquilla, arXiv e-prints, arXiv:2003.11040 (2020), arXiv:2003.11040 [physics.comp-ph].
 - [12] L. Wang, *Phys. Rev. B* **94**, 195105 (2016).
 - [13] J. Carrasquilla and R. G. Melko, *Nature Physics* **13**, 431 (2017).
 - [14] E. P. L. van Nieuwenburg, Y.-H. Liu, and S. D. Huber, *Nature Physics* **13**, 435 (2017).
 - [15] Y. Zhang and E.-A. Kim, *Phys. Rev. Lett.* **118**, 216401 (2017).
 - [16] K. Ch’ng, J. Carrasquilla, R. G. Melko, and E. Khatami, *Phys. Rev. X* **7**, 031038 (2017).
 - [17] B. S. Rem, N. Käming, M. Tarnowski, L. Asteria, N. Fläschner, C. Becker, K. Sengstock, and C. Weitenberg, *Nature Physics* **15**, 917 (2019).
 - [18] A. Bohrdt, C. S. Chiu, G. Ji, M. Xu, D. Greif, M. Greiner, E. Demler, F. Grusdt, and M. Knap, *Nature Physics* **15**, 921 (2019).
 - [19] Y. Zhang, A. Mesaros, K. Fujita, S. D. Edkins, M. H. Hamidian, K. Ch’ng, H. Eisaki, S. Uchida, J. C. S. Davis, E. Khatami, and E.-A. Kim, *Nature* **570**, 484–490 (2019).
 - [20] G. Carleo and M. Troyer, *Science* **355**, 602 (2017).
 - [21] D.-L. Deng, X. Li, and S. Das Sarma, *Phys. Rev. X* **7**, 021021 (2017).
 - [22] M. H. Amin, E. Andriyash, J. Rolfe, B. Kulchitsky, and R. Melko, *Phys. Rev. X* **8**, 021050 (2018).
 - [23] M. Schmitt and M. Heyl, arXiv e-prints, arXiv:1912.08828 (2019), arXiv:1912.08828 [cond-mat.str-el].
 - [24] S. J. Wetzel, *Phys. Rev. E* **96**, 022140 (2017).
 - [25] K. Ch’ng, N. Vazquez, and E. Khatami, *Phys. Rev. E* **97**, 013306 (2018).
 - [26] W. Hu, R. R. P. Singh, and R. T. Scalettar, *Phys. Rev. E* **95**, 062122 (2017).
 - [27] N. C. Costa, W. Hu, Z. J. Bai, R. T. Scalettar, and R. R. P. Singh, *Phys. Rev. B* **96**, 195138 (2017).
 - [28] J. F. Rodriguez-Nieva and M. S. Scheurer, *Nature Physics* **15**, 790 (2019).
 - [29] Y. Long, J. Ren, and H. Chen, *Phys. Rev. Lett.* **124**, 185501 (2020).
 - [30] E. A.-C. Elena Lopez, Adrien Scheuer and F. Chinesta, *Mathematics and Mechanics of Complex Systems* **6**, 251–265 (2018).
 - [31] E. Facco, A. Pagnani, E. T. Russo, and A. Laio, *PLOS Computational Biology* **15**, 1 (2019).
 - [32] N. Krueger and M. Felsberg, in *Proceedings of the British Machine Vision Conference* (BMVA Press, 2003) pp. 27.1–27.10.
 - [33] A. A. Ramos, H. Socas-Navarro, A. L. Ariste, and M. M. González, *The Astrophysical Journal* **660**, 1690 (2007).
 - [34] A. Ansuini, A. Laio, J. H. Macke, and D. Zoccolan, in *Advances in Neural Information Processing Systems* (2019) pp. 6109–6119.
 - [35] D. C. Laughlin, *Journal of Ecology* **102**, 186 (2014).
 - [36] S. Wold, K. Esbensen, and P. Geladi, *Chemometrics and Intelligent Laboratory Systems* **2**, 37 (1987).
 - [37] I. Borg and P. J. Groenen, *Modern multidimensional scaling: Theory and applications* (Springer Science & Business Media, 2005).
 - [38] M. Balasubramanian and E. L. Schwartz, *Science* **295**, 7 (2002).
 - [39] S. T. Roweis and L. K. Saul, *Science* **290**, 2323 (2000).
 - [40] L. v. d. Maaten and G. Hinton, *Journal of machine learning research* **9**, 2579 (2008).

- [41] L. McInnes, J. Healy, and J. Melville, arXiv e-prints , arXiv:1802.03426 (2018), [arXiv:1802.03426 \[stat.ML\]](#).
- [42] F. Camastra and A. Vinciarelli, IEEE Transactions on pattern analysis and machine intelligence **24**, 1404 (2002).
- [43] D. Stauffer and A. Aharony, Introduction To Percolation Theory (London: Taylor and Francis, 1991).
- [44] U. Wolff, *Phys. Rev. Lett.* **62**, 361 (1989).
- [45] D. P. Landau and K. Binder, [A Guide to Monte Carlo Simulations in Statistical Physics](#) (Cambridge: Cambridge University Press, 2005).
- [46] P. Di Francesco, P. Mathieu, and D. Sénéchal, [Conformal field theory](#), Graduate texts in contemporary physics (Springer, New York, NY, 1997).
- [47] M. Henkel, [Conformal Invariance and Critical Phenomena](#) (Springer, Berlin, Heidelberg, 1999).
- [48] F. Y. Wu, *Rev. Mod. Phys.* **54**, 235 (1982).
- [49] S. Iino, S. Morita, N. Kawashima, and A. W. Sandvik, *Journal of the Physical Society of Japan* **88**, 034006 (2019).
- [50] J. M. Kosterlitz and D. J. Thouless, *Journal of Physics C: Solid State Physics* **6**, 1181 (1973).
- [51] R. Gupta, J. DeLapp, G. G. Batrouni, G. C. Fox, C. F. Baillie, and J. Apostolakis, *Phys. Rev. Lett.* **61**, 1996 (1988).
- [52] Y.-D. Hsieh, Y.-J. Kao, and A. W. Sandvik, *Journal of Statistical Mechanics: Theory and Experiment* **2013**, P09001 (2013).
- [53] A. W. Sandvik, *AIP Conference Proceedings* **1297**, 135 (2010).
- [54] C. Wang and H. Zhai, *Phys. Rev. B* **96**, 144432 (2017).
- [55] M. J. S. Beach, A. Golubeva, and R. G. Melko, *Phys. Rev. B* **97**, 045207 (2018).
- [56] A. Lidiak and Z. Gong, arXiv e-prints , arXiv:2003.07399 (2020), [arXiv:2003.07399 \[quant-ph\]](#).
- [57] Q. Hoan Tran, M. Chen, and Y. Hasegawa, arXiv e-prints , arXiv:2004.03169 (2020), [arXiv:2004.03169 \[cond-mat.stat-mech\]](#).
- [58] D. R. Nelson and J. M. Kosterlitz, *Phys. Rev. Lett.* **39**, 1201 (1977).
- [59] E. Buddenoir and S. Wallon, *Journal of Physics A: Mathematical and General* **26**, 3045 (1993).
- [60] M. E. Fisher and A. N. Berker, *Phys. Rev. B* **26**, 2507 (1982).
- [61] K. Binder and D. P. Landau, *Phys. Rev. B* **30**, 1477 (1984).
- [62] A. Rodriguez, M. d’Errico, E. Facco, and A. Laio, *Journal of Chemical Theory and Computation* **14**, 1206 (2018).
- [63] M. d’Errico, E. Facco, A. Laio, and A. Rodriguez, arXiv e-prints , arXiv:1802.10549 (2018), [arXiv:1802.10549 \[stat.ML\]](#).
- [64] C. Gross and I. Bloch, [Annual Review of Cold Atoms and Molecules](#), Chap. 4, pp. 181–199.
- [65] E. Khatami, E. Guardado-Sanchez, B. M. Spar, J. F. Carrasquilla, W. S. Bakr, and R. T. Scalettar, arXiv e-prints , arXiv:2002.12310 (2020), [arXiv:2002.12310 \[cond-mat.str-el\]](#).